ACS NANO

www.acsnano.org

ARTICLE

Exciton Dynamics in MoS_2-Pentacene and WSe_2-Pentacene Heterojunctions

Pavel A. Markeev,* Emad Najafidehaghani, Gergely F. Samu, Krisztina Sarosi, Sirri Batuhan Kalkan, Ziyang Gan, Antony George, Veronika Reisner, Karoly Mogyorosi, Viktor Chikan, Bert Nickel, Andrey Turchanin, and Michel P. de Jong

Cite This: *ACS Nano* 2022, 16, 16668–16676

Read Online

ACCESS | Metrics & More | Article Recommendations | Supporting Information

ABSTRACT: We measured the exciton dynamics in van der Waals heterojunctions of transition metal dichalcogenides (TMDCs) and organic semiconductors (OSs). TMDCs and OSs are semiconducting materials with rich and highly diverse optical and electronic properties. Their heterostructures, exhibiting van der Waals bonding at their interfaces, can be utilized in the field of optoelectronics and photovoltaics. Two types of heterojunctions, MoS_2-pentacene and WSe_2-pentacene, were prepared by layer transfer of 20 nm pentacene thin films as well as MoS_2 and WSe_2 monolayer crystals onto Au surfaces. The samples were studied by means of transient absorption spectroscopy in the reflectance mode. We found that A-exciton decay by hole transfer from MoS_2 to pentacene occurs with a characteristic time of 21 ± 3 ps. This is slow compared to previously reported hole transfer times of 6.7 ps in MoS_2-pentacene junctions formed by vapor deposition of pentacene molecules onto MoS_2 on SiO_2. The B-exciton decay in WSe_2 shows faster hole transfer rates for WSe_2-pentacene heterojunctions, with a characteristic time of 7 ± 1 ps. The A-exciton in WSe_2 also decays faster due to the presence of a pentacene overlayer; however, fitting the decay traces did not allow for the unambiguous assignment of the associated decay time. Our work provides important insights into excitonic dynamics in the growing field of TMDC-OS heterojunctions.

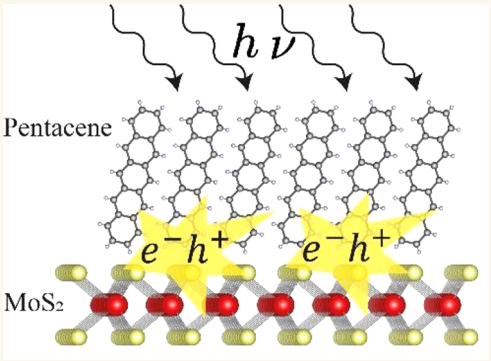

KEYWORDS: *transition metal dichalcogenides, organic semiconductors, pentacene, exciton dynamics, transient reflection spectroscopy, MoS_2, WSe_2*

1. INTRODUCTION

The study of van der Waals heterojunctions based on transition metal dichalcogenides (TMDCs) and organic semiconductor (OS) thin films has been ongoing for several years; however, there are still many fascinating avenues for researchers to explore.[1] The TMDCs themselves exhibit fascinating physical phenomena such as exceptionally large exciton binding energies,[2,3] spin-valley locking,[4] and the exciton Hall effect.[5] TMDCs and organic semiconductors are highly dissimilar nonconventional semiconductors that share the characteristic of interlayer bonding via van der Waals interactions. Forming heterojunctions of these materials offers interesting opportunities for combining diverse (opto-)electronic properties. An important step for the technological development of such structures has been taken recently, in the demonstration by some of us of devices fabricated by layer transfer of TMCDs as well as organic semiconductor thin films.[6] A strong advantage of this approach is that the organic semiconductors can be grown on a suitable substrate for obtaining high quality crystalline layers, avoiding molecular disorder that occurs upon direct deposition on TMCD substrates.

The wide variety of devices that have been constructed in the field so far include light emitting diodes,[7] tunneling transistors,[8] and photovoltaic cells.[9,10] Arguably, one of the most promising applications out of these possibilities is photovoltaics, and the present work is carried out in its context, focusing on exciton dynamics at TMDC/OS interfaces. Some of the aforementioned heterojunctions have been studied previously in various combinations and conditions by similar ultrafast pump probe spectroscopic techniques.[10−16] Most of these previous studies focused on 2D TMDCs grown on quartz and SiO_2/Si wafers, which were then

Received: June 22, 2022
Accepted: September 28, 2022
Published: September 30, 2022

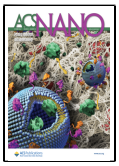

covered by an OS layer directly deposited onto the TMDC monolayers. TMDCs such as MoS_2 and WSe_2 monolayers have attracted a lot of attention as promising 2D semiconductors and have been studied thoroughly.[17−20] Here, we examine high quality monolayers of MoS_2 and WSe_2 prepared by a dedicated chemical vapor deposition (CVD) technique and transferred to a UV ozone treated Au substrate.[21−23] Homogeneous pentacene films, 20 nm in thickness, were also transferred to the samples after uniform controlled growth on poly(acrylic acid) (PAA) substrate films.[6]

Transient absorption/reflection spectroscopy (TAS/TRS) is a well-known technique to study ultrafast processes of exciton formation and dissociation in various materials.[12,24,25] Even though the performance of photovoltaic devices is based on many different aspects, one of these is the temporal difference between exciton decay and charge separation on the junction interface. Recently, relatively long lasting (5.1 ns) charge-separated states at MoS_2-pentacene interfaces have been reported.[15] In this work, pentacene was directly grown on the surface of MoS_2, while MoS_2 was deposited on the substrate by a CVD method similar to ours. Here, we focus on the ultrafast exciton dynamics in van der Waals heterojunctions of WSe_2 and MoS_2 monolayer crystals covered by a 20 nm transferred thin film of pentacene. This allows us to investigate to which extent molecular (dis)order at the MoS_2/pentacene interface affects exciton dissociation rates. Charge transfer dynamics at WSe_2/pentacene interfaces have not been studied previously.

2. RESULTS AND DISCUSSION

Here, the obtained TRS results are presented in the following manner. First, we discuss the pentacene reflection spectra. Next, TRS results of MoS_2 and MoS_2-pentacene heterojunctions are presented, with analysis and conclusions. Lastly, the ultrafast spectroscopic analysis of the results of WSe_2 and WSe_2-pentacene composites are presented and discussed.

Figure 1 shows the structural arrangement of pentacene molecules on MoS_2. We expect highly oriented vertically

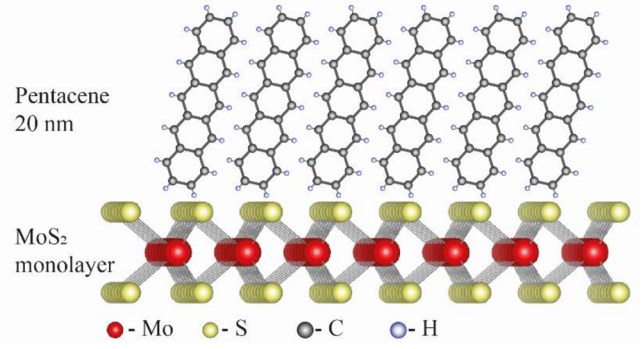

Figure 1. Structural arrangement of pentacene on MoS_2.

packed pentacene molecules at the interface with the TMDC monolayer. The same arrangement is expected for the WSe_2-pentacene sample. Photoemission electron microscopy (PEEM) images of similar samples, showing the crystalline nature of the pentacene layer, can be found in Figure S6 in the Supporting Information.

2.1. Pentacene. Figure 2a shows two-dimensional (2D) absorption spectra (average of measurements taken at three different locations) on a 20 nm thin film of pentacene transferred to gold. The sample is photoexcited at 515 nm, and the transient reflectivity spectra are recorded. ΔOD_R is calculated as $-\log(I_{R,exc}/I_{R,noexc})$ where $I_{R,exc}$ and $I_{R,noexc}$ are the reflected light intensity with and without excitation, respectively. The temporal resolution of the experiment is 80 fs. The spectra are dominated by a strong ground state bleach feature, attributed to the depopulation of the ground state by the pump pulse. This feature is centered at 688 nm and corresponds to the lowest energy singlet exciton in pentacene. Two weaker bleach signals are recognizable at 635 and 597 nm. The spectrum recorded at a pump−probe delay time of 0.53 ps can be found in the inset of Figure 2b. These results are in good agreement with previously published works on (transient) optical absorption spectroscopy of (poly)crystalline pentacene.[25−27] The separation between the 688 nm (1.80 eV) and 635 nm (1.95 eV) peaks can be attributed to the Davydov splitting due to the presence of two inequivalent pentacene molecules in the unit cell.[27]

Figure 2b shows the kinetic trace extracted at the main bleach feature of the pentacene film (integrated signal intensity from 675 to 695 nm). The data show that the ground state bleach is long-lived and hardly evolves within 1 ns after excitation. Note that ultrafast (sub 150 fs) fission of singlet excitons into two triplet excitons, which is known to be an efficient process in pentacene,[25,26] is not detectable on the comparatively long time scales probed in our measurements.

2.2. Molybdenum Disulfide (MoS_2). Figure 2c,d shows transient reflection spectra for uncovered MoS_2 single crystals on Au (Figure 2c), as well as MoS_2 monolayer crystals on Au that are covered by a 20 nm continuous film of pentacene (Figure 2d). There are two main ground state bleach peaks observed for the MoS_2 single crystals, centered at 615 nm and at 662 nm. These values represent the B- and A-excitons of MoS_2, respectively. The decay processes that these excitons undergo in similar samples (i.e., MoS_2 monolayers on amorphous SiO_2, quartz and sapphire) have been thoroughly studied previously.[20,28−30] For pentacene-covered MoS_2 (see Figure 2d and Figure 3), two partially overlapping ground state bleach features appear at about 670 nm, which are attributed to the MoS_2 A-exciton and the closely located pentacene bleach peak at 688 nm.

Figure 3 shows the transient reflection spectra of three different samples: the MoS_2 monolayer in blue, pentacene in green, and the MoS_2 crystal covered with the pentacene thin film in orange. These spectra were captured 0.53 ps after photoexcitation. As was discussed earlier, pentacene has three main bleach peaks, and MoS_2 has two, while the intense pentacene ground state bleach at 688 nm is located very close to the MoS_2 A-exciton peak. In the MoS_2-pentacene data, one can observe a composite feature that results from the superposition of the two individual peaks.

To study the mechanism(s) of exciton decay in the kinetic traces and to provide quantitative comparison of the various samples, we fitted the data with a triple exponential decay function as shown below:

$$\Delta OD_R = A_1 \times \exp\left(-\frac{t}{t_1}\right) + A_2 \times \exp\left(-\frac{t}{t_2}\right) + A_3 \times \exp\left(-\frac{t}{t_3}\right) \quad (1)$$

https://doi.org/10.1021/acsnano.2c06144
ACS Nano 2022, 16, 16668−16676

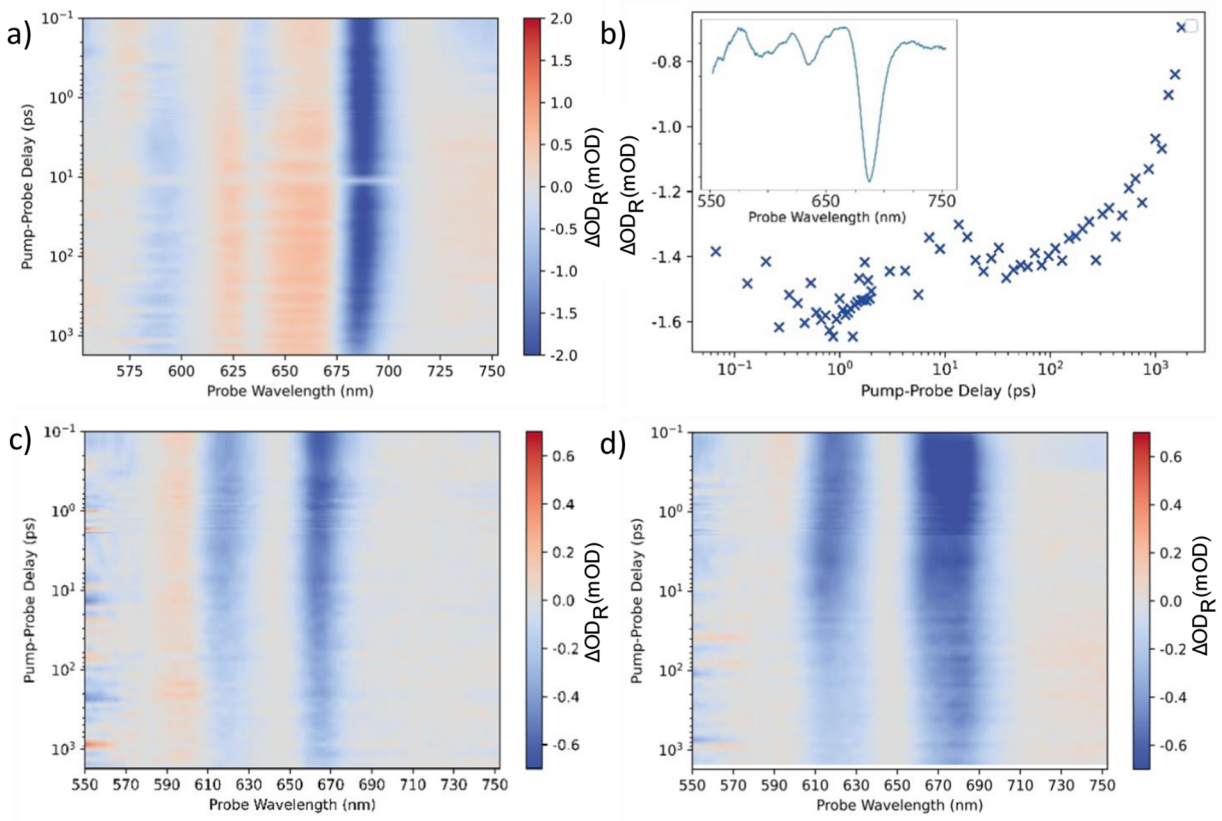

Figure 2. (a) Two-dimensional transient reflection spectra of a 20 nm pentacene film on a gold substrate. Here and further the background subtraction (described in Supporting Information 2) is applied to this type of result. (b) A kinetic trace of the main feature at 675−695 nm from the averaged spectra in (a); inset represents the spectrum at 0.53 ps delay time. (c, d) Two-dimensional transient reflection spectra of (c) MoS_2 monolayer crystals transferred to a gold substrate and (d) similar MoS_2 monolayer crystals on gold covered by a pentacene thin film.

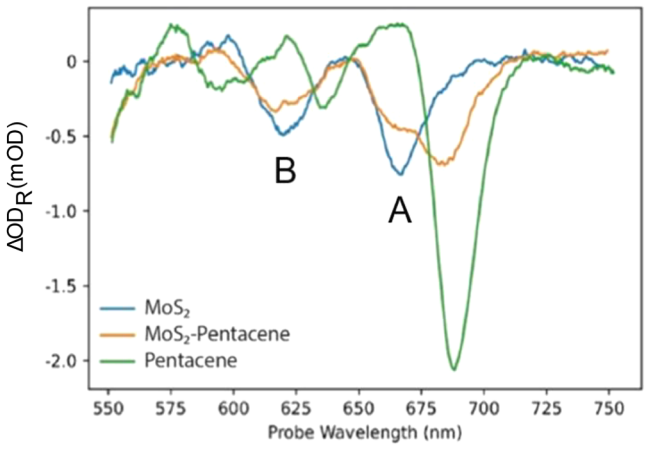

Figure 3. Transient reflection spectra of a MoS_2 monolayer, a MoS_2-pentacene junction, and a pentacene thin film (all on Au substrates) probed at 0.53 ps.

The results of this fitting can be seen in Figure 4a, corresponding to the kinetic trace of the A-exciton of MoS_2. The fast decay component of the A-exciton in uncovered MoS_2 crystals was fitted to be 1.0 ± 0.5 ps. This component is usually attributed to fast trapping processes of excitons at intrinsic defect sites such as atomic S- and S_2-vacancies,[15,29,31,32] and/or to exciton cooling effects.[33−35] The second component of 28.3 ± 9.4 ps represents the nonradiative decay of exciton−phonon pairs.[30,32] The slow component of 1.9 ± 0.3 ns is usually associated with the lifetime of free charges[35] and their radiative recombination.[36,37] The fractional weight of each decay component is presented in Table 1 next to the values of the decay times.

For the MoS_2-pentacene heterojunction results, we follow a similar fitting method applied by Homan *et al.*,[15] in which decay components that are not affected by the presence of pentacene are fixed, such as ultrafast defect-assisted decay and the slow decay components. The new intermediate component, with a decay time of 21 ± 3 ps, then is associated with the hole transfer from pentacene to the MoS_2 crystal (see ref 15 for schematic diagrams illustrating the corresponding decay processes). This new component accounts for 34% of the fit, to be compared to the previous intermediate fraction of 26%. We were not able to detect any new component associated with slow recombination processes of transferred holes with excess electrons in MoS_2 on the scale of a few nanoseconds, which most probably fall outside our time window of 2 ns used in the experiments. The exciton decay characteristics of MoS_2 crystals covered by the pentacene thin film are found to be quite similar to those of uncovered MoS_2. Notably, the time scale for exciton dissociation at the MoS_2-pentacene interface of 21 ± 3 ps is slow compared to the previously reported hole transfer time of 6.7 ps for pentacene grown on MoS_2 on SiO_2/Si.[15] The decay process of the B-exciton, which is presented in Figure 4b, is similarly not significantly affected by the presence of the pentacene film: All the fitted decay components (see

https://doi.org/10.1021/acsnano.2c06144
ACS Nano 2022, 16, 16668−16676

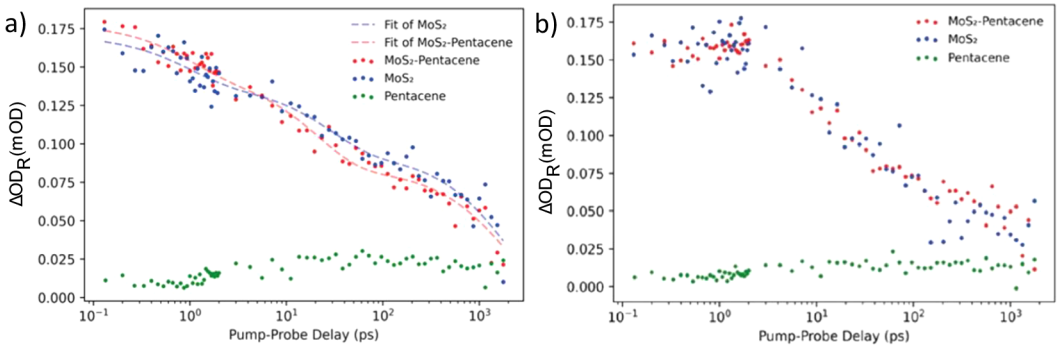

Figure 4. Normalized decay traces of MoS_2 excitons in a MoS_2 monolayer compared to those in a MoS_2-pentacene junction, both on gold substrates. (a) A-exciton probed at 665 nm, fitted by a three-exponential decay function; (b) B-exciton probed at 615 nm.

Table 1. Fit Parameters for Decay Traces of A-Excitons in Composite MoS_2 and MoS_2-Pentacene Samples[a]

	t_1 [ps] (A1)	t_2 [ps] (A2)	t_3 [ps] (A3)	t_4 [ps] (A4)
	carrier trapping	h^+ transfer	exciton–phonon scattering	radiative recombination and e^- trapping
MoS_2 single crystal	1.0 ± 0.5 (19%)		28 ± 9 (27%)	1900 ± 265 (54%)
MoS_2-pentacene heterojunction	**1.0** (18%)	21 ± 3 (34%)		**1900** (48%)

[a]Bold values are fixed during the fit for the heterojunction.

Supporting Information) are very similar and agree within the error bar for both the MoS_2 and MoS_2-pentacene samples in our measurements. Figure 4b shows the data without fitted time traces, and the overlapping data sets clearly show the same type of behavior for both systems.

There are several possible explanations for the different exciton dynamics in our MoS_2-pentacene samples fabricated by layer transfer as compared to the observations of Homan *et al.*[15] The pentacene layers grown by physical vapor deposition on water-soluble poly(acrylic acid) are highly crystalline, as has been confirmed by X-ray diffraction measurements performed on similar samples both before and after layer transfer.[6] Consequently, the MoS_2-pentacene interface features pentacene molecules that are "standing up" as they would on the

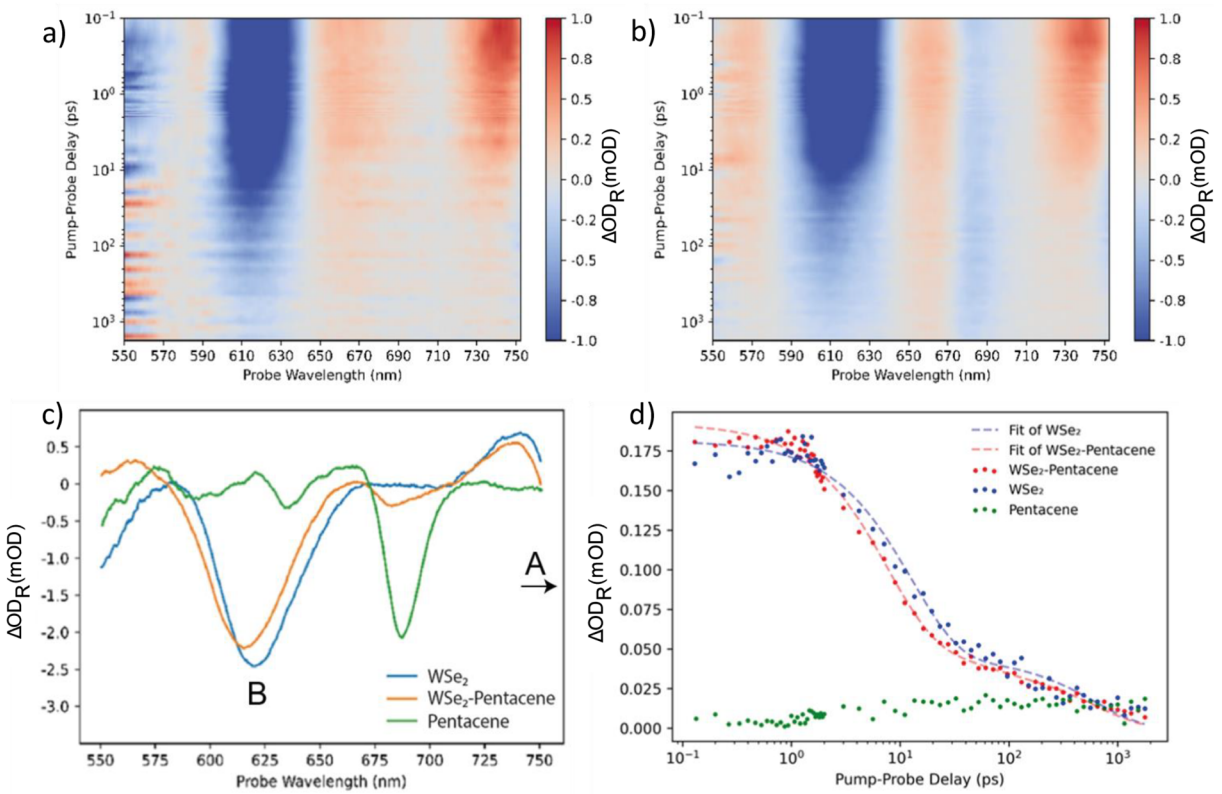

Figure 5. Transient reflection spectra of (a) WSe_2 monolayer crystals transferred to a gold substrate and (b) WSe_2 monolayer crystals covered by a pentacene thin film on the same substrate. A pentacene bleach peak appears at 688 nm in (b). (c) Transient reflection spectra of WSe_2 monolayer, WSe_2-pentacene junction and pentacene thin film, all on gold substrates, probed at 0.53 ps. (d) Normalized decay traces of B-excitons in a WSe_2 monolayer compared to a WSe_2-pentacene junction probed at 618 nm, both on gold substrates.

https://doi.org/10.1021/acsnano.2c06144
ACS Nano 2022, 16, 16668–16676

growth substrate. In contrast, disordered MoS_2-pentacene interfaces formed by physical vapor deposition of pentacene on MoS_2[15] are expected to exhibit molecules that are more randomly oriented, including molecules that are lying flat on the substrate. Several experimental studies indeed have shown that molecular monolayers of pentacene deposited onto MoS_2 comprise molecules that adopt such an orientation on the surface.[38,39] Since exciton dissociation by hole transfer relies on the electronic coupling between the π- and π^*-orbitals of pentacene and the MoS_2 bands, the increased overlap of the electronic wave functions for molecules that are lying flat on MoS_2 would indeed give rise to faster exciton decay.

In addition, the substrates on which the MoS_2-pentacene layers reside may play a role. Our MoS_2-pentacene heterojunctions were transferred onto gold substrates, while in the work of Homan *et al.* quartz substrates were used. For MoS_2 gold interfaces, Fermi level pinning has been observed by us previously.[40] According to a recent publication,[41] the bandgap of MoS_2 and WSe_2 is also somewhat affected by the substrate: The band gap of MoS_2 is decreased by 0.21 eV and that of WSe_2 by 0.16 eV when the monolayers are located on Au substrates. These effects might lead to a different alignment of MoS_2 and pentacene energy levels as compared to MoS_2-pentacene heterojunctions on insulating quartz substrates. Huang *et al.* reported that the presence of a gold substrate modifies the charge distribution in MoS_2.[42] All of the above could affect the hole transfer rates at the MoS_2/pentacene interface. We would like to stress, however, that in our experiments we used UV/ozone-treated Au substrates exhibiting a thin surface oxide, which decreases the aforementioned effects of gold on the TMDC monolayers significantly. For a strongly coupled Au/MoS_2 system, photoexcited states in MoS_2 could decay via interactions with the gold substrate,[43] which then could affect the exciton decay behavior in samples both with and without pentacene. Since the exciton decay dynamics observed for our Au/MoS_2 samples are quite similar to the findings of Homan *et al.*, who studied MoS_2 on SiO_2, this mechanism most probably does not play a major role in our experiments, and it can be concluded that the coupling between Au and MoS_2 is rather weak.

2.3 Tungsten Diselenide (WSe_2). The second part of our work is dedicated to tungsten diselenide (WSe_2) monolayer crystals compared to WSe_2-pentacene heterojunctions. The pentacene layer is nominally the same as in the case of MoS_2: a 20 nm thick continuous film. The WSe_2 and pentacene layers again have been transferred onto a gold substrate. Our TRS measurements of WSe_2 single crystals, shown in Figure 5a, show a bleach peak at 610 nm for the B-exciton and a positive signal near the expected wavelength of the A-exciton above 730 nm. The peak position of the B-exciton is in agreement with previous publications.[18,19] The positive signal might be related to a photoinduced absorption feature of an excited state. In addition, excitonic features could sometimes produce positive signals instead of bleaching due to broadening of the absorption spectra after excitation by the pump pulse.[44] The positive signal appears at the border of the studied spectral window, and hence its temporal evolution cannot be traced accurately. Figure 5b shows TRS data for the WSe_2-pentacene junction. Besides the just discussed features of WSe_2, one can easily recognize a bleach peak of pentacene at 688 nm.

Figure 5c shows the TRS spectra of a WSe_2 monolayer (orange) and a WSe_2-pentacene heterojunction (green), as well as a pentacene thin film (all on Au substrates). The spectra are recorded at 0.53 ps after excitation of the system by the pump pulse. The B-exciton peak is experiencing a slight blue shift in the presence of pentacene, to 615 nm from 621 nm for the WSe_2-only sample. The observed shift might be related to a reduction of the exciton binding energy due to screening effects, as has been predicted for WSe_2 encapsulated by hexagonal boron nitride.[45]

The most interesting region of the measured TRS data is associated with the B-excitons of WSe_2 as was mentioned earlier. In this section, we repeat the same procedure of fitting an exponential decay function described above to WSe_2 B-excitons for the two different samples. The exciton behavior in monolayer crystals of WSe_2 is not as well studied as is the case for MoS_2. A number of previous works focused attention on A- and C-excitons in few layer and bulk WSe_2, mostly studying the ultrafast component <1 ps.[17−20] He *et al.*[46] provide some information on lifetimes of excitons in WSe_2 monolayers. For the uncovered WSe_2 monolayer, the decay traces of the B-excitons in our TRS measurements are well described by just two exponential components (see Figure 5d). Using a two exponential fit is not a unique way of studying the decay dynamics in TMDC monolayers and has been already implemented previously in work on $MoSe_2$ monolayers.[47] We do not detect a sub-picosecond decay component corresponding to ultrafast carrier trapping associated with defects in the single crystal, as found for MoS_2. Previously, we reported that similarly prepared monolayers of WSe_2 on metallic substrates feature vacuum level alignment according to the Schottky−Mott limit, unlike MoS_2 layers for which Fermi level pinning is observed.[40] This different energy level alignment points to a considerably lower defect density in WSe_2 as compared to MoS_2, consistent with the absence of ultrafast defect-assisted trapping. The obtained values for t_2 and t_3 are 12 ± 1 ps and 624 ± 112 ps. The latter component corresponds to one-quarter of the weight in the biexponential fit. The decay traces of the WSe_2-pentacene heterojunction require an extra component with t_1 equal to 7 ± 1 ps to obtain a good fit, which we attribute to hole transfer from pentacene to WSe_2. In the WSe_2-pentacene case, t_2 (12 ps) is kept fixed; keeping both t_2 and t_3 or only t_3 fixed did not provide any reasonable fitting results. It should be noted, however, that similar values for t_3 as well as the weights of the slow decay component are found in the case of the heterojunction and uncovered WSe_2 case.

In addition, the decay of A-excitons in WSe_2 was measured with a silicon detector using spectral filters only, by means of lock-in detection resulting in better S/N in the data while losing some spectral resolution. The filter used to obtain the data is a FB700-40, i.e., with a 40 nm range centered at 700 nm (Supporting Information 1). Using this filter is suitable for

Table 2. Fit Parameters for Decay Traces of B-Excitons in WSe_2/WSe_2-Pentacene Samples[a]

	t_1 [ps] (A1)	t_2 [ps] (A2)	t_3 [ps] (A3)
	h^+ transfer	exciton−phonon scattering	radiative recombination and e^- trapping
WSe_2 single crystal		12 ± 1 (75%)	624 ± 112 (25%)
WSe_2-pentacene heterojunction	7 ± 1 (39%)	**12 (40%)**	705 ± 95 (20%)

[a]Bold values are fixed during the fit for the heterojunction.

https://doi.org/10.1021/acsnano.2c06144
ACS Nano 2022, 16, 16668−16676

Table 3. Fit Parameters for Decay Traces of A-Excitons in WSe_2/WSe_2-Pentacene Samples

	t_1 [ps] (A1)	t_2 [ps] (A2)	t_3 [ps] (A3)	t_4 [ps] (A4)
WSe_2 single crystal	8.1 ± 0.9 (56%)		32.2 ± 5.6 (24%)	401.4 ± 34.8 (20%)
WSe_2-pentacene heterojunction	6.6 ± 1.3 (54%)	17.3 ± 4.9 (29%)		125.1 ± 11.3 (17%)

detecting the temporal evolution of the A-exciton signal because even though it covers a rather large portion of the spectrum, there is no (ultra)fast decay of other excited states, e.g., of pentacene, which could negatively impact the data, such that the information that we obtain derives from the A-excitons in WSe_2. The behavior of the A-exciton is noticeably different from that of the B-exciton presented earlier. The decay trace of the uncovered WSe_2 layer was fitted with a three exponential decay function comprising fast (8 ± 1 ps), intermediate (32 ± 6 ps), and slow (401 ± 35 ps) components. Again, an ultrafast sub-picosecond component is absent as in the case of the WSe_2 B-exciton. The graph representing the fitting result can be found in the Supporting Information (Figure S7).

It turned out that it was not possible to follow a similar method for fitting for the decay trace of the WSe_2-pentacene heterojunction as in the previous cases because fixing any of the components resulted in a poor fit of the data. The fast component t_1 in the WSe_2-pentacene case decreased by about 20% to 6.6 ± 1.3 ps. A new component with a t_2 of 17.3 ± 4 ps is attributed to the TMDC-pentacene interactions. Interestingly, the slow component decreased by more than a factor of 3 and became 125.1 ± 11.3, while the weight in the fit is almost not affected and stays at around one-fifth in both cases. Because of the new manner of fitting without any fixed components, we do not assign the time components to known processes as was done previously.

The different behavior of the A- versus B-excitons might indicate a different formation and decay process of the B-exciton compared to the A-exciton, possibly related to the different excitation energies and the availability of different decay channels. Previous work on WS_2 and WSe_2 also showed different decay dynamics for these exciton species.[48] Another work showed a significant difference in differential transmission of A- and B-excitons in MoS_2, which is explained by spectral Γ broadening. This also explains the amplitude difference for these two excitons.[28] Noticeable differences in photoluminescence emission (intensity and profiles) of A- and B-excitons were reported and connected to the sample's defect density.[49]

3. CONCLUSION

We studied exciton dynamics in van der Waals heterojunctions of MoS_2-pentacene and WSe_2-pentacene. We have found that in the case of MoS_2-pentacene heterojunctions the presence of the pentacene film has a moderate influence on the decay kinetics of A- and B-excitons. The A exciton was mostly affected by the presence of the pentacene film, exhibiting a 21 ± 3 ps decay component associated with hole transfer from MoS_2 to pentacene. Our results are noticeably different compared to a previous report on a similar structure, i.e., pentacene grown on MoS_2 on SiO_2,[15] showing a faster hole transfer on the time scale of 6.7 ps. Several factors contribute to this, in particular, the different molecular orientations in transferred versus vapor deposited pentacene films, and the utilization of a different substrate (gold in this work versus SiO_2 substrate). The exciton dynamics could be affected by a different energy level alignment at the MoS_2-pentacene interface, due to the Fermi level of MoS_2 being pinned to that of the gold substrate.[40] In the case of WSe_2-pentacene heterojunctions, the A- and B-excitons showed different decay schemes. The B-exciton signal of the WSe_2 monolayer was fitted with a two-exponential decay function, with 12 and 624 ps components. In the presence of pentacene, the best fit was obtained by adding a fast 7 ps component associated with hole transfer, while keeping the 12 ps component fixed and changing the slow component to 705 ps. The A exciton decay was best described by fitting of a three-exponential decay function. The presence of pentacene again resulted in overall faster decay of the WSe_2 A-exciton. It was however not possible to assign individual decay components unambiguously to known processes because fixing the decay components did not provide reasonable fits. We believe that our results on TMDC-OS heterojunctions will help to stimulate future research and technical advancements in the area.

4. METHODS AND MATERIALS

MoS_2 and WSe_2 monolayer single crystals were grown on thermally oxidized silicon substrates (Siltronix, oxide thickness 300 nm, roughness <0.2 nm RMS) by a modified CVD growth method in which a Knudsen-type effusion cell is used for the delivery of sulfur and selenium precursors.[21,23]

For heterostructure fabrication, the as-grown TMDs were transferred onto a suitable gold substrate. We have employed a poly(methyl methacrylate) (PMMA) assisted transfer protocol for the transfer.[21] A PMMA layer of 200 nm (950 kDa, Allresist GmbH, AR-P 679.04) was spin coated onto the SiO_2/Si substrate with CVD grown TMD crystals. Then the substrate was kept floating on top of a bath of KOH solution (85%, Carl Roth) to etch away the SiO_2 layer and to release the TMD crystals supported by PMMA followed by washing several times with ultrapure water (18.2 MΩcm, Membrapure) to remove any residual KOH. Then the PMMA supported monolayer TMD was placed on the target substrate and baked at 90 °C for 10 min, followed by immersion in acetone for 2 h to remove the PMMA support, followed by rinsing with isopropyl alcohol.

A 50 nm thick poly(acrylic acid) (PAA) layer was spin coated on a borosilicate glass substrate as water-soluble sacrificial layer. Then, 20 nm thick pentacene was evaporated on PAA with a deposition rate of 0.1 Å s^{-1}, while the substrate was held at room temperature. After the pentacene deposition, the highly ordered organic nanosheet was delaminated by dissolving the PAA layer by side injection of water from a reservoir.[6] The floating nanosheet was transferred to a DI beaker to ease the transfer onto the target substrate. In parallel, the target substrate with transferred MoS_2 was immersed into acetone for 2 h to remove the PMMA supporting layer prior to nanosheet transfer. Then, the floating nanosheet was picked up by the target substrate and carefully dried under ambient conditions.

The process of transient absorption/reflectivity spectroscopy was conducted by a dedicated system at the research institute ELI-ALPS (Szeged, Hungary). The setup consists of a high speed (2000 spectra/s) fiber optic spectrometer and a laser driving the experiments. The laser system is a few-optical cycle ytterbium fiber chirped-pulse amplifier system that generates 30 fs pulses, with a 100 μJ pulse energy, at a repetition rate of 100 kHz centered at 1030 nm. The schematic layout, a more detailed description, and validation experiment of the custom-built transient absorption/reflection spectrometer are described in Supporting Information 1. The generated laser pulse is split into a 80/20 ratio where 80% of the

https://doi.org/10.1021/acsnano.2c06144
ACS Nano 2022, 16, 16668−16676

beam is used for the pump beam generation, and the remaining 20% generates the probe beam. The pump beam is frequency doubled on a Type-I BBO crystal (Eksma optics, 2 mm) resulting in a 515 nm center wavelength pulse. The pump-beam was focused on the sample surface with an excitation fluence of 0.7 mJ cm^{-2}. The probe beam was focused on the sample surface into a 60 μm × 50 μm spot with a 10 μJ cm^{-2} fluence ensuring that the probe beam focus was smaller than the pump beam focus for optimal signal levels.

The obtained data were processed by a specially tuned Python script for background subtraction (Supporting Information 2). Spectral regions between the bleach peaks were adopted as reference points according to which background was subtracted appropriately. An example of the raw versus processed data, as well as the code, can be found in Supporting Information 2. The transient reflection spectra in images 3 and 6 were not additionally processed. Decay kinetic traces were obtained by direct averaging over a specified wavelength window without additional processing. The process of fitting the three-exponential decay function to study the exciton decay constants was compiled in a Python script utilizing the sklearn library including a least-squares error method.

ASSOCIATED CONTENT

Supporting Information

The Supporting Information is available free of charge at https://pubs.acs.org/doi/10.1021/acsnano.2c06144.

Experimental details of transient absorption/reflection spectroscopy, transient reflection spectra of mechanically exfoliated MoS_2 for validation of the setup, a description of Python scripts for data processing, and fits of decay traces of B-excitons in MoS_2 and MoS_2-pentacene samples (PDF)

AUTHOR INFORMATION

Corresponding Author

Pavel A. Markeev − *MESA+ Institute for Nanotechnology, University of Twente, 7500 AE Enschede, The Netherlands;* orcid.org/0000-0002-5445-1224; Email: p.markeev@utwente.nl

Authors

Emad Najafidehaghani − *Institute of Physical Chemistry, Abbe Center of Photonics, Friedrich Schiller University, 07743 Jena, Germany*

Gergely F. Samu − *ELI-ALPS, ELI-HU Non-Profit Ltd., Szeged H-6728, Hungary;* orcid.org/0000-0002-3239-9154

Krisztina Sarosi − *ELI-ALPS, ELI-HU Non-Profit Ltd., Szeged H-6728, Hungary*

Sirri Batuhan Kalkan − *Faculty of Physics and CeNS, Ludwig-Maximilians-Universität, 80539 Munich, Germany*

Ziyang Gan − *Institute of Physical Chemistry, Abbe Center of Photonics, Friedrich Schiller University, 07743 Jena, Germany*

Antony George − *Institute of Physical Chemistry, Abbe Center of Photonics, Friedrich Schiller University, 07743 Jena, Germany;* orcid.org/0000-0002-9317-5920

Veronika Reisner − *Faculty of Physics and CeNS, Ludwig-Maximilians-Universität, 80539 Munich, Germany*

Karoly Mogyorosi − *ELI-ALPS, ELI-HU Non-Profit Ltd., Szeged H-6728, Hungary*

Viktor Chikan − *ELI-ALPS, ELI-HU Non-Profit Ltd., Szeged H-6728, Hungary; Department of Chemistry, Kansas State University, Manhattan, Kansas 66506-0401, United States;* orcid.org/0000-0002-4157-3556

Bert Nickel − *Faculty of Physics and CeNS, Ludwig-Maximilians-Universität, 80539 Munich, Germany;* orcid.org/0000-0002-0254-8841

Andrey Turchanin − *Institute of Physical Chemistry, Abbe Center of Photonics, Friedrich Schiller University, 07743 Jena, Germany;* orcid.org/0000-0003-2388-1042

Michel P. de Jong − *MESA+ Institute for Nanotechnology, University of Twente, 7500 AE Enschede, The Netherlands;* orcid.org/0000-0003-3668-9121

Complete contact information is available at: https://pubs.acs.org/10.1021/acsnano.2c06144

Notes

The authors declare no competing financial interest.

ACKNOWLEDGMENTS

The authors acknowledge financial support by the European Union's Horizon 2020 Research and Innovation Program FLAG-ERA JTC 2017, managed by the Dutch Research Council (NWO) under Grant No. 680-91-313 and the Deutsche Forschungsgemeinschaft (DFG) under Contract No. NI 632/6-1 and Grant TU149/9-1 (#397373225). The Jena group received financial support from the Deutsche Forschungsgemeinschaft (DFG) through a Research Infrastructure Grant INST 275/257-1 FUGG (#313713174), CRC 1375 NOA (Project B2, #398816777), and SPP2244 (Project TU149/13-1, #443361515). B.N. acknowledges support from the Bavarian State Ministry of Science, Research and Arts, through the grant "Solar Technologies Go Hybrid (SolTech)". The ELI ALPS project (GINOP-2.3.6-15-2015-00001) is supported by the European Union and co-financed by the European Regional Development Fund.

REFERENCES

(1) Jariwala, D.; Marks, T. J.; Hersam, M. C. Mixed-Dimensional van Der Waals Heterostructures. *Nat. Mater.* **2017**, 170−181, DOI: 10.1038/nmat4703.

(2) Joe, A. Y.; Jauregui, L. A.; Pistunova, K.; Mier Valdivia, A. M.; Lu, Z.; Wild, D. S.; Scuri, G.; De Greve, K.; Gelly, R. J.; Zhou, Y.; Sung, J.; Sushko, A.; Taniguchi, T.; Watanabe, K.; Smirnov, D.; Lukin, M. D.; Park, H.; Kim, P. Electrically Controlled Emission from Singlet and Triplet Exciton Species in Atomically Thin Light-Emitting Diodes. *Phys. Rev. B* **2021**, *103*, 161411.

(3) Chernikov, A.; Berkelbach, T. C.; Hill, H. M.; Rigosi, A.; Li, Y.; Aslan, O. B.; Reichman, D. R.; Hybertsen, M. S.; Heinz, T. F. Exciton Binding Energy and Nonhydrogenic Rydberg Series in Monolayer WS2. *Phys. Rev. Lett.* **2014**, *113* (7), 076802.

(4) Mak, K. F.; He, K.; Shan, J.; Heinz, T. F. Control of Valley Polarization in Monolayer MoS2 by Optical Helicity. *Nat. Nanotechnol.* **2012**, *7* (8), 494−498.

(5) Onga, M.; Zhang, Y.; Ideue, T.; Iwasa, Y. Exciton Hall Effect in Monolayer MoS2. *Nat. Mater.* **2017**, *16* (12), 1193−1197.

(6) Kalkan, S. B.; Najafidehaghani, E.; Gan, Z.; Apfelbeck, F. A. C.; Hübner, U.; George, A.; Turchanin, A.; Nickel, B. Wafer Scale Synthesis of Organic Semiconductor Nanosheets for van Der Waals Heterojunction Devices. *NPJ. 2D Mater. Appl.* **2021**, *5* (1), 1−6.

(7) Withers, F.; Del Pozo-Zamudio, O.; Mishchenko, A.; Rooney, A. P.; Gholinia, A.; Watanabe, K.; Taniguchi, T.; Haigh, S. J.; Geim, A. K.; Tartakovskii, A. I.; Novoselov, K. S. Light-Emitting Diodes by Band-Structure Engineering in van Der Waals Heterostructures. *Nat. Mater.* **2015**, *14* (3), 301−306.

(8) Lin, Y. C.; Ghosh, R. K.; Addou, R.; Lu, N.; Eichfeld, S. M.; Zhu, H.; Li, M. Y.; Peng, X.; Kim, M. J.; Li, L. J.; Wallace, R. M.; Datta, S.; Robinson, J. A. Atomically Thin Resonant Tunnel Diodes Built from

Synthetic van Der Waals Heterostructures. *Nat. Commun.* **2015**, *6*, 7311 DOI: 10.1038/ncomms8311.
(9) Furchi, M. M.; Pospischil, A.; Libisch, F.; Burgdörfer, J.; Mueller, T. Photovoltaic Effect in an Electrically Tunable Van Der Waals Heterojunction. *Nano Lett.* **2014**, *14* (8), 4785−4791.
(10) Petoukhoff, C. E.; Krishna, M. B. M.; Voiry, D.; Bozkurt, I.; Deckoff-Jones, S.; Chhowalla, M.; O'Carroll, D. M.; Dani, K. M. Ultrafast Charge Transfer and Enhanced Absorption in MoS2-Organic van Der Waals Heterojunctions Using Plasmonic Metasurfaces. *ACS Nano* **2016**, *10* (11), 9899−9908.
(11) Liu, X.; Gu, J.; Ding, K.; Fan, D.; Hu, X.; Tseng, Y. W.; Lee, Y. H.; Menon, V.; Forrest, S. R. Photoresponse of an Organic Semiconductor/Two-Dimensional Transition Metal Dichalcogenide Heterojunction. *Nano Lett.* **2017**, *17* (5), 3176−3181.
(12) Zhu, T.; Yuan, L.; Zhao, Y.; Zhou, M.; Wan, Y.; Mei, J.; Huang, L.Highly Mobile Charge-Transfer Excitons in Two-Dimensional WS_2/Tetracene Heterostructures. *Sci. Adv.***2018**, *4* (1). DOI: 10.1126/sciadv.aao3104.
(13) Kafle, T. R.; Kattel, B.; Lane, S. D.; Wang, T.; Zhao, H.; Chan, W. L. Charge Transfer Exciton and Spin Flipping at Organic-Transition-Metal Dichalcogenide Interfaces. *ACS Nano* **2017**, *11* (10), 10184−10192.
(14) Gobbi, M.; Orgiu, E.; Samorì, P. When 2D Materials Meet Molecules: Opportunities and Challenges of Hybrid Organic/Inorganic van Der Waals Heterostructures. *Adv. Mater.* **2018**, *30* (18), 1706103.
(15) Homan, S. B.; Sangwan, V. K.; Balla, I.; Bergeron, H.; Weiss, E. A.; Hersam, M. C. Ultrafast Exciton Dissociation and Long-Lived Charge Separation in a Photovoltaic Pentacene-MoS2 van Der Waals Heterojunction. *Nano Lett.* **2017**, *17* (1), 164−169.
(16) Zhao, B.; Gan, Z.; Johnson, M.; Najafidehaghani, E.; Rejek, T.; George, A.; Fink, R. H.; Turchanin, A.; Halik, M.; Zhao, B.; Rejek, T.; Halik, M.; Gan, Z.; Najafidehaghani, E.; George, A.; Turchanin, A.; Johnson, M.; Fink, R. H. 2D van Der Waals Heterojunction of Organic and Inorganic Monolayers for High Responsivity Phototransistors. *Adv. Funct Mater.* **2021**, *31* (42), 2105444.
(17) Steinleitner, P.; Merkl, P.; Nagler, P.; Mornhinweg, J.; Schüller, C.; Korn, T.; Chernikov, A.; Huber, R. Direct Observation of Ultrafast Exciton Formation in a Monolayer of WSe2. *Nano Lett.* **2017**, *17* (3), 1455−1460.
(18) Xing, X.; Zhao, L.; Zhang, W.; Wang, Z.; Su, H.; Chen, H.; Ma, G.; Dai, J.; Zhang, W. Influence of a Substrate on Ultrafast Interfacial Charge Transfer and Dynamical Interlayer Excitons in Monolayer WSe2/Graphene Heterostructures. *Nanoscale* **2020**, *12* (4), 2498−2506.
(19) Cui, Q.; Ceballos, F.; Kumar, N.; Zhao, H. Transient Absorption Microscopy of Monolayer and Bulk WSe2. *ACS Nano* **2014**, *8* (3), 2970−2976.
(20) Valencia-Acuna, P.; Zereshki, P.; Tavakoli, M. M.; Park, J. H.; Kong, J.; Zhao, H. Transient Absorption of Transition Metal Dichalcogenide Monolayers Studied by a Photodope-Pump-Probe Technique. *Phys. Rev. B* **2020**, *102* (3), 2−8.
(21) George, A.; Neumann, C.; Kaiser, D.; Mupparapu, R.; Lehnert, T.; Hübner, U.; Tang, Z.; Winter, A.; Kaiser, U.; Staude, I.; Turchanin, A. Controlled Growth of Transition Metal Dichalcogenide Monolayers Using Knudsen-Type Effusion Cells for the Precursors. *JPhys. Materials* **2019**, *2* (1), 016001.
(22) Shree, S.; George, A.; Lehnert, T.; Neumann, C.; Benelajla, M.; Robert, C.; Marie, X.; Watanabe, K.; Taniguchi, T.; Kaiser, U.; Urbaszek, B.; Turchanin, A. High Optical Quality of MoS2Monolayers Grown by Chemical Vapor Deposition. *2d Mater.* **2020**, *7* (1), 015011.
(23) Najafidehaghani, E.; Gan, Z.; George, A.; Lehnert, T.; Ngo, G. Q.; Neumann, C.; Bucher, T.; Staude, I.; Kaiser, D.; Vogl, T.; Hübner, U.; Kaiser, U.; Eilenberger, F.; Turchanin, A. 1D p−n Junction Electronic and Optoelectronic Devices from Transition Metal Dichalcogenide Lateral Heterostructures Grown by One-Pot Chemical Vapor Deposition Synthesis. *Adv. Funct Mater.* **2021**, *31*, 2101086.
(24) Berera, R.; van Grondelle, R.; Kennis, J. T. M. Ultrafast Transient Absorption Spectroscopy: Principles and Application to Photosynthetic Systems. *Photosynth Res.* **2009**, *101* (2−3), 105−118.
(25) Wilson, M. W. B.; Rao, A.; Clark, J.; Kumar, R. S. S.; Brida, D.; Cerullo, G.; Friend, R. H. Ultrafast Dynamics of Exciton Fission in Polycrystalline Pentacene. *J. Am. Chem. Soc.* **2011**, *133* (31), 11830−11833.
(26) Broch, K.; Dieterle, J.; Branchi, F.; Hestand, N. J.; Olivier, Y.; Tamura, H.; Cruz, C.; Nichols, V. M.; Hinderhofer, A.; Beljonne, D.; Spano, F. C.; Cerullo, G.; Bardeen, C. J.; Schreiber, F. Robust Singlet Fission in Pentacene Thin Films with Tuned Charge Transfer Interactions. *Nat. Commun.* **2018**, *9* (1), 954 DOI: 10.1038/s41467-018-03300-1.
(27) Cocchi, C.; Breuer, T.; Witte, G.; Draxl, C. Polarized Absorbance and Davydov Splitting in Bulk and Thin-Film Pentacene Polymorphs. *Phys. Chem. Chem. Phys.* **2018**, *20* (47), 29724−29736.
(28) Sim, S.; Park, J.; Song, J. G.; In, C.; Lee, Y. S.; Kim, H.; Choi, H. Exciton Dynamics in Atomically Thin MoS2: Interexcitonic Interaction and Broadening Kinetics. *Phys. Rev. B Condens Matter Mater. Phys.* **2013**, *88* (7), 1−5.
(29) Cunningham, P. D.; McCreary, K. M.; Hanbicki, A. T.; Currie, M.; Jonker, B. T.; Hayden, L. M. Charge Trapping and Exciton Dynamics in Large-Area CVD Grown MoS2. *J. Phys. Chem. C* **2016**, *120* (10), 5819−5826.
(30) Wang, H.; Zhang, C.; Rana, F. Ultrafast Dynamics of Defect-Assisted Electron−Hole Recombination in Monolayer MoS 2. *Nano Lett.* **2015**, *15* (1), 339−345.
(31) George, A.; Fistul, M. V.; Gruenewald, M.; Kaiser, D.; Lehnert, T.; Mupparapu, R.; Neumann, C.; Hübner, U.; Schaal, M.; Masurkar, N.; Arava, L. M. R.; Staude, I.; Kaiser, U.; Fritz, T.; Turchanin, A. Giant Persistent Photoconductivity in Monolayer MoS2 Field-Effect Transistors. *NPJ. 2D Mater. Appl.* **2021**, *5* (1), 1−8.
(32) Shi, H.; Yan, R.; Bertolazzi, S.; Brivio, J.; Gao, B.; Kis, A.; Jena, D.; Xing, H. G.; Huang, L. Exciton Dynamics in Suspended Monolayer and Few-Layer MoS2 2D Crystals. *ACS Nano* **2013**, *7* (2), 1072−1080.
(33) Czech, K. J.; Thompson, B. J.; Kain, S.; Ding, Q.; Shearer, M. J.; Hamers, R. J.; Jin, S.; Wright, J. C. Measurement of Ultrafast Excitonic Dynamics of Few-Layer MoS2 Using State-Selective Coherent Multidimensional Spectroscopy. *ACS Nano* **2015**, *9* (12), 12146−12157.
(34) Nie, Z.; Long, R.; Sun, L.; Huang, C. C.; Zhang, J.; Xiong, Q.; Hewak, D. W.; Shen, Z.; Prezhdo, O. V.; Loh, Z. H. Ultrafast Carrier Thermalization and Cooling Dynamics in Few-Layer MoS2. *ACS Nano* **2014**, *8* (10), 10931−10940.
(35) Tsokkou, D.; Yu, X.; Sivula, K.; Banerji, N. The Role of Excitons and Free Charges in the Excited-State Dynamics of Solution-Processed Few-Layer MoS2 Nanoflakes. *J. Phys. Chem. C* **2016**, *120* (40), 23286−23292.
(36) Palummo, M.; Bernardi, M.; Grossman, J. C. Exciton Radiative Lifetimes in Two-Dimensional Transition Metal Dichalcogenides. *Nano Lett.* **2015**, *15* (5), 2794−2800.
(37) Korn, T.; Heydrich, S.; Hirmer, M.; Schmutzler, J.; Schuller, C. Low-Temperature Photocarrier Dynamics in Monolayer MoS2. *Appl. Phys. Lett.* **2011**, *99* (10), 102109.
(38) Tumino, F.; Rabia, A.; Bassi, A. L.; Tosoni, S.; Casari, C. S. Interface-Driven Assembly of Pentacene/MoS2Lateral Heterostructures. *J. Phys. Chem. C* **2022**, *126* (2), 1132−1139.
(39) Kachel, S. R.; Dombrowski, P. M.; Breuer, T.; Gottfried, J. M.; Witte, G. Engineering of TMDC-OSC Hybrid Interfaces: The Thermodynamics of Unitary and Mixed Acene Monolayers on MoS2. *Chem. Sci.* **2021**, *12* (7), 2575−2585.
(40) Markeev, P. A.; Najafidehaghani, E.; Gan, Z.; Sotthewes, K.; George, A.; Turchanin, A.; de Jong, M. P. Energy-Level Alignment at Interfaces between Transition-Metal Dichalcogenide Monolayers and Metal Electrodes Studied with Kelvin Probe Force Microscopy. *J. Phys. Chem. C* **2021**, *125* (24), 13551−13559.
(41) Park, S.; Mutz, N.; Schultz, T.; Blumstengel, S.; Han, A.; Aljarb, A.; Li, L. J.; List-Kratochvil, E. J. W.; Amsalem, P.; Koch, N. Direct

Determination of Monolayer MoS2 and WSe2 Exciton Binding Energies on Insulating and Metallic Substrates. *2d Mater.* **2018**, *5* (2), 025003.
(42) Huang, Y.; Pan, Y. H.; Yang, R.; Bao, L. H.; Meng, L.; Luo, H. L.; Cai, Y. Q.; Liu, G. D.; Zhao, W. J.; Zhou, Z.; Wu, L. M.; Zhu, Z. L.; Huang, M.; Liu, L. W.; Liu, L.; Cheng, P.; Wu, K. H.; Tian, S. B.; Gu, C. Z.; Shi, Y. G.; Guo, Y. F.; Cheng, Z. G.; Hu, J. P.; Zhao, L.; Yang, G. H.; Sutter, E.; Sutter, P.; Wang, Y. L.; Ji, W.; Zhou, X. J.; Gao, H. J. Universal Mechanical Exfoliation of Large-Area 2D Crystals. *Nat. Commun.* **2020**, *11* (1), 2453.
(43) Camellini, A.; Mazzanti, A.; Mennucci, C.; Martella, C.; Lamperti, A.; Molle, A.; Buatier de Mongeot, F.; Della Valle, G.; Zavelani-Rossi, M. Evidence of Plasmon Enhanced Charge Transfer in Large-Area Hybrid Au−MoS2Metasurface. *Adv. Opt Mater.* **2020**, *8* (24), 2000653.
(44) Aleithan, S. H.; Livshits, M. Y.; Khadka, S.; Rack, J. J.; Kordesch, M. E.; Stinaff, E. Broadband Femtosecond Transient Absorption Spectroscopy for a CVD Mo S2Monolayer. *Phys. Rev. B* **2016**, *94* (3), 1−7.
(45) Gerber, I. C.; Marie, X. Dependence of Band Structure and Exciton Properties of Encapsulated WSe2Monolayers on the HBN-Layer Thickness. *Phys. Rev. B* **2018**, *98* (24), 245126.
(46) He, C.; Zhu, L.; Zhao, Q.; Huang, Y.; Yao, Z.; Du, W.; He, Y.; Zhang, S.; Xu, X. Competition between Free Carriers and Excitons Mediated by Defects Observed in Layered WSe2 Crystal with Time-Resolved Terahertz Spectroscopy. *Adv. Opt Mater.* **2018**, *6* (19), 1800290.
(47) Hao, S.; Bellus, M. Z.; He, D.; Wang, Y.; Zhao, H. Controlling Exciton Transport in Monolayer MoSe2 by Dielectric Screening. *Nanoscale Horiz* **2020**, *5* (1), 139−143.
(48) Eroglu, Z. E.; Contreras, D.; Bahrami, P.; Azam, N.; Mahjouri-Samani, M.; Boulesbaa, A. Filling Exciton Trap-States in Two-Dimensional Tungsten Disulfide (Ws2) and Diselenide (Wse2) Monolayers. *Nanomaterials* **2021**, *11* (3), 1−11.
(49) McCreary, K. M.; Hanbicki, A. T.; Sivaram, S. V.; Jonker, B. T. A- and B-Exciton Photoluminescence Intensity Ratio as a Measure of Sample Quality for Transition Metal Dichalcogenide Monolayers. *APL Mater.* **2018**, *6* (11), 111106.

https://doi.org/10.1021/acsnano.2c06144
ACS Nano 2022, 16, 16668−16676